A parallel multidomain strategy to compute turbulent flows in fan-stirred closed vessels

A. Bonhomme [a,*], F. Duchaine [c], G. Wang [d,1], L. Selle [a,b], T. Poinsot [a,b]

[a] Université de Toulouse, INPT, UPS, IMFT (Institut de Mécanique des Fluides de Toulouse), Allée Camille Soula, F-31400 Toulouse, France
[b] CNRS, IMFT, F-31400 Toulouse, France
[c] CERFACS, GlobC Team, 42 Avenue Gaspard Coriolis, 31057 Toulouse Cedex 01, France
[d] CERFACS, CFD Team, 42 Avenue Gaspard Coriolis, 31057 Toulouse Cedex 01, France

A B S T R A C T

This paper presents a parallel multidomain strategy to compute the turbulent flow in a closed vessel stirred by six fans. The method is based on running multiple instances of the same solver, working on different subdomains and communicating through small overlapping zones where interpolations allow to handle moving meshes. First the accuracy of this Multi Instances Solver Coupled on Overlapping Grids (MISCOG) approach is evaluated for the convection of a single vortex. Load balancing issues on parallel machines are discussed and a performance model is proposed to allocate cores to each code instance. Then, the method is applied to the LES of a closed vessel stirred by six fans. Mean and fluctuating fields obtained by the LES are compared to experimental data. Finally, the structure of the turbulence generated at the center of the vessel is studied and the mechanisms allowing turbulence to travel from the fans to the center of the vessel are analyzed.

Keywords:
Code coupling
Fan-stirred vessel
Homogeneous isotropic turbulence
Turbulent flame speed

1. Introduction

Turbulence has been studied for decades in its most canonical form: homogeneous isotropic turbulence (HIT) [1–7]. This limit case is the cornerstone of multiple theoretical approaches as well as the building brick of Large Eddy Simulation (LES) models where the Kolmogorov cascade assumption allows to model the effects of small scales from information available for the resolved ones [8,9]. HIT is also the only generic case where the interaction of other phenomena with turbulence can be defined using a limited number of parameters: evolution of large droplets in HIT [10–12], interaction of evaporating droplets with HIT [13], flame/turbulence interaction [14–16].

While defining HIT theoretically or numerically is a reasonably simple and clear task, creating HIT experimentally is more challenging. This paper focuses on one classical technique used to generate HIT: fan-stirred closed vessels. Sometimes these apparatus are called 'bombs', a denomination that will be used in this paper. Stirring vessels with fans to study turbulent flame propagation has been used for more than a century (see Laffitte's book [17]). A classical paper where this turbulence was qualified as HIT is due to Semenov [18] who showed that properly designed bombs with multiple fans were able to generate reasonable HIT in a zone located near the center of the chamber where the mean flow is almost zero and turbulence is homogeneous and isotropic. A significant amount of work has been based on correlations obtained in such bombs. The most famous example is probably the quest for 'turbulent flame speed' correlations in which the speed s_T of premixed turbulent flames is expressed as a function of the initial turbulent velocity u'. Such correlations continue to be frequently published [19–23] and interestingly, few of them agree. One reason for this may be that the notion of a generic turbulent flame speed depending only on a limited number of flow and flame parameters may not be relevant [14]. Another one could be that the initial turbulence in such bombs is not really close to HIT and that more parameters should be taken into account. Therefore, since most models are based on measurements performed in bombs, an interesting question is to study whether the flow created in a fan-stirred bomb really mimics HIT and over which spatial extent. This question has been investigated experimentally [18,24,25] but using CFD would be a useful addition.

Even though the largest CFD simulations to date have been published for HIT with meshes up to 64 billion points [26], all of them were performed in simple cubic meshes, initialized with a flow which has all the properties of theoretical HIT. None of these

* Corresponding author. Tel.: +33 0534322893.
E-mail addresses: adrien.bonhomme@imft.fr (A. Bonhomme), laurent.selle@imft.fr (L. Selle), thierry.poinsot@imft.fr (T. Poinsot).
[1] Now at Sherbrooke University.

simulations address the question of how HIT is created (if it is) in a real fan-stirred bomb. This question is much more complicated and existing experimental diagnostics are not always sufficient to guaranty that the flow in this situation matches all properties of theoretical HIT: in a bomb, fans obviously induce a strong mean, pulsated flow. In the center of the vessel, the mean flow is expected to be zero and turbulence assumed to diffuse to a central zone where HIT is expected. This involves a series of questions which are rarely addressed:

- By which mechanisms does turbulence transfer from the fan region to the central zone?
- Since the number of fans is usually limited, are there preferential straining axes in the bomb which could affect isotropy near its center?
- The fans flow being by nature unsteady, is turbulence at the center of the apparatus sensitive to the pulsating nature of the flow created by the blades rotation?
- How large is the zone where HIT is obtained?

The objective of this paper is to show how the turbulent flow in a fan-stirred vessel can be studied using high-resolution LES to complement experimental diagnostics. To reach this objective, the simulation code must satisfy three criteria:

- Considering the complexity of the objects to mesh, the need to correctly capture the blade geometry and the necessity to handle moving objects, unstructured meshes are required so that classical DNS codes used for HIT (spectral methods [27,28], high-order compact schemes [29–31]) cannot be used.
- The configuration includes a large number of moving objects (the fans) close to each other. Classical techniques such as ALE (Arbitrary Lagrangian Eulerian) [32–34] are difficult to implement for a flow with multiple fans because of meshing issues. Immersed Boundary methods [35–37] are easier to develop for moving objects but are usually associated to a low order of accuracy which is not acceptable in a LES framework. Here, a new multidomain high-order LES technique with mesh overlapping developed by Wang et al. [38,39] is used on a real configuration.
- To resolve turbulent structures accurately, a high-fidelity explicit (in time) LES solver is needed and the corresponding CPU cost is expected to be large so that the implementation of the multidomain method must be fully parallel.

This paper is organized as follows: first, the numerical methodology is described in Section 2. It is based on the simultaneous execution of multiple instances of the same solver, called MISCOG for Multi Instances Solver Coupled on Overlapping Grids. These instances are coupled on parallel computers using the OpenPalm coupler [40,41]. This coupler is well suited for this task, however, one limitation is that only two instances can exchange at the same time so that the balancing strategy becomes much more complex than it was for a single instance, which is also discussed in Section 2.

A validation test case of the MISCOG approach is presented in Section 3. It consists in propagating a single vortex across two overlapping computational domains. It is thought as an elementary validation of the ability to convect turbulent structures. The method is then applied to a fan-stirred bomb experiment developed in Orléans [42], where 7 instances are required to compute the bomb and the six fans. Section 4 describes this configuration, the numerical set-up and the parallel efficiency of the global simulation.

Flow results are discussed in Section 5: quantities that can be obtained both from LES and PIV are first compared (mean flow fields and RMS values for all three velocity components). LES results are used to analyze quantities which cannot be obtained experimentally such as the velocity tensor – to identify the structure of the turbulence – or the budget of turbulent kinetic energy in order to understand how turbulence reaches the center of the vessel.

2. Numerical methodology

The filtered LES unsteady compressible Navier–Stokes equations that describe the spatially filtered mass, momentum and energy conservation are solved by the unstructured compressible LES solver, AVBP [43]. These equations can be written in the conservative form:

$$\frac{\partial \mathbf{W}}{\partial t} + \vec{\nabla} \cdot \vec{\mathbf{F}} = 0 \tag{1}$$

where $\mathbf{W}$ is the vector containing the conservative variables $(\rho, \rho U, \rho E)^T$ and $\vec{\mathbf{F}} = (\mathbf{F}, \mathbf{G}, \mathbf{H})^T$ is the flux tensor. The flux is divided into two components: the convective flux depending only on $\mathbf{W}$ and the viscous flux depending on both $\mathbf{W}$ and its gradient $\nabla\mathbf{W}$. The contributions of Sub-Grid Scale (SGS) turbulence models are included in the viscous flux through the addition of the so called turbulent viscosity ν_t. Two schemes are used in this study: Lax–Wendroff [44] (LW, with 2nd-order accuracy in time and space) and the two-step Taylor–Galerkin finite element scheme TTGC [45] (3rd-order in time and space). The LW scheme, which is faster than TTGC is used for transient phases while all statistics are gathered (when steady state is reached) using the TTGC scheme.

To compute the whole configuration and the flow created by the fans the code must be able to deal with moving parts (in this case, six rotating fans). Immersed Boundaries Methods [35,36] were tested but were not able to represent correctly the blade geometry of the fan because the entire zone spanned by the fans must be meshed with a very fine grid size leading to a prohibitive cost in term of CPU time. ALE methods with mesh deformation [46,47,34] were also considered but introduced excessive deformation of cells and frequent interpolation phases [48].

To solve this problem, the MISCOG approach, developed initially for turbomachinery [38,39], was extended to bomb configurations. In MISCOG, two or more instances of the same LES solver (namely AVBP), each with their own computational domain, are coupled through the parallel coupler OpenPALM [40,41]. For the bomb case, the whole flow domain is initially divided into 7 parts: the bomb itself has a static mesh (AVBP01) while each fan is computing in a moving framework (AVBP0i, $i \in [2;7]$). For moving parts, the code uses the ALE block rotation approach [46,47,34]: the grid is rotated without deformation. The remaining unit AVBP01 simulates the flow in the static part of the bomb in the same coordinate system. The solution retained to handle interfaces between the units involving rotating and non-rotating parts consists in reconstructing the residuals using an overset grid method and exchanging by interpolation the multidomain conservative variables wherever needed. To do so an efficient distributed search algorithm is implemented in the OpenPALM coupler to locate the points in parallel partitioned mesh blocks and a linear method is used to interpolate residuals (the interpolation is of 2nd order). This coupling phase is implemented outside the CFD instances in conjunction with second order interpolation.

The computational domain corresponding to the experiment of Orléans is displayed in Fig. 1: six cylindrical rotating domains ($i = 2$–7) are used for each fan zone while one domain ($i = 1$) is used for the rest of the bomb. In general, the number of cells used for each domain can be different. Here the grids for the six fans (AVBP02–AVBP07) have the same number of cells but the bomb

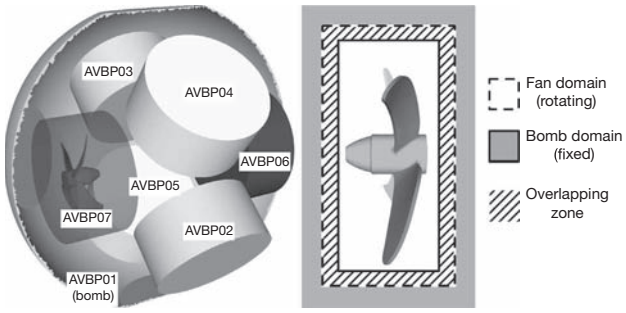

Fig. 1. MISCOG decomposition for a fan-stirred vessel. Six cylindrical rotating domains (AVBP02–AVBP07) for the fans and one fixed domain (AVBP01) for the rest of the bomb.

grid (AVBP01) is different so that load balancing becomes immediately an issue which will be discussed in Section 4.2. The timetable used in the MISCOG approach for each iteration is the following:

1. All AVP0i ($i \in [1;N]$) entities run.
2. When AVBP01 and AVBP02 have computed one iteration, they exchange conservative variables in the buffer zone of regions 1 and 2. After this exchange, AVBP02 starts to compute the next iteration.
3. When AVBP03 finishes its iteration and AVBP01 has also finished exchanging with AVBP02, AVBP01 and AVBP03 start to exchange, otherwise AVBP01 waits. This is repeated for all AVBP0i instances ($i \in [2;N]$).

Note that AVBP01 starts to compute the next iteration as soon as it has exchanged residuals with the last instance AVBP0N.

3. Validation test cases

Many academic test cases have been performed to validate the MISCOG approach in configurations where a single domain computation or an analytical solution can be used as the reference solution. For example, acoustic wave and two-dimensional vortex propagation cases were tested successfully using MISCOG by Wang et al. [38,39]. These results showed good performances of the MISCOG approach and a negligible accuracy loss through the overlapping zone thanks to the second-order interpolation. Here a new three-dimensional vortex case closer to the Orléans bomb geometry was tested by propagating a vortex with the TTGC scheme in the box of Fig. 2.

The computational domain consists in a tri-periodic cubic box where a cylindrical grid is inserted. This cylinder is rotated at 10,000 rpm corresponding to the rotation speed of the fans in the real bomb. The mean flow goes from left to right at U_0. In this test case, the vortex must travel through interfaces without being affected by the inner rotating mesh so that the exact solution is simple to derive as a reference. This test case is representative of the target configuration where fans are encapsulated in finite cylinders: vortices created by the fan blades must travel through the coupling interface. This case is simulated both with the MISCOG approach and with a single domain AVBP computation. Fig. 3(a) presents the time evolution of the axial velocity at the center of the rotating cylinder while Fig. 3(b) shows a cut of the pressure field after two convection times. A very good agreement is found between the analytical solution, the single domain computation and the MISCOG approach. The vortex is convected at the expected speed U_0 (no dispersion) and its structure is preserved (no dissipation). Note that formally, when the vortex goes through the overlapping zone, the third order of the TTGC scheme is lost since the current interpolation is of 2nd order. However, the pressure and the velocity profiles are both well convected.

This test case demonstrates the ability of the MISCOG approach to convect a 3D vortex through different interfaces and confirms the accuracy of this approach for coupled LES. On the long term, it is clear that the interpolation method used in the overlapping zone combined with the numerical scheme in each domain leads to global dispersion and dissipation properties which would require a much more precise analysis. This is left for further studies to concentrate here on the fan-stirred bomb simulations.

4. Numerical set-up and parallel efficiency of the MISCOG approach on a six-fan stirred vessel

This section describes the bomb configuration and the numerical set-up. The parallel efficiency of the global MISCOG simulation is discussed because it raises new questions compared to classical load balancing issues in a single instance solver.

4.1. Description of the bomb configuration and numerical set-up

The configuration is the bomb experiment of the PRISME laboratory in Orléans [42]. This spherical vessel is stirred by six fans. The radius of the closed vessel R_0 is 100 mm and it has six windows for visualization (see Fig. 4(a)). Fans are axial fans with an external diameter of 60 mm. All characteristics of the fans are presented by Fig. 4(b).

Simulations used to gather statistics are performed with the TTGC scheme. The sub-grid scale (SGS) model is WALE [49] which was developed for wall bounded flows. All boundary conditions are no-slip and adiabatic walls (fans and closed vessel).

Experimental results obtained in the PRISME laboratory, give values for the RMS velocity $\mathbf{u}_{\mathbf{rms},\mathrm{exp}}$ and the integral length scale $L_{\tau,exp}$ at the bomb center: $\mathbf{u}_{\mathbf{rms},\mathrm{exp}} \simeq 3$ m/s and $L_{\tau,exp} \simeq 3$ mm. The time scale associated to the integral length scale τ is $\tau = L_{\tau,exp}/\mathbf{u}_{rms,exp} \simeq 1$ ms. Knowing the viscosity $\nu = 1.78.10^{-5}$ m^2 s^{-1} the turbulent Reynolds number can be evaluated $Re_{t,exp} = \mathbf{u}_{\mathbf{rms},\mathrm{exp}} L_{\tau,exp}/\nu \simeq 600$. The experimental Kolmogorov length scale η_{exp} can be estimated with the relation:

$$\eta_{exp} = L_{\tau,exp}/Re_{t,exp}^{3/4} \tag{2}$$

giving a value of the order of $\eta_{exp} \simeq 40$ μm. All theses information are summarized in Table 1. The computation with a constant mesh size in the whole bomb of $\Delta x = 1$ mm in the closed vessel gives a ratio $\Delta x/\eta_{exp} \simeq 25$ corresponding to a mesh of 21 million of cells for AVBP01. Even though the computation is a LES, this resolution leads almost to a DNS-like computation because very few intense structures actually exist between the Kolmogorov scale η and a length of the order of 20η [5]. For the mesh of the fan, a fine discretization at the blade-walls is used to capture the flow generated by fans (Fig. 5): four prism layers are added on all blade-walls to describe the boundary layer [50]. The typical thickness of the prism layers is about 0.05 mm, so that the maximum wall $y+$[2] on the first grid point near the blade wall is 10 and is located at the leading edge of the blade (see Fig. 6). The mesh size around the fan (away from the walls) is 1 mm leading to a mesh of 3.3 million cells for each fan instance AVBP02 to AVBP07. Thus the full mesh including the bomb-mesh and the six fan-meshes contains 41 million cells.

[2] The normalized wall distance y^+ is defined by $u^+ = yu_\tau/\nu$ where u_τ is the friction velocity. u_τ is defined by $u_\tau = \sqrt{\tau_{wall}/\rho}$.

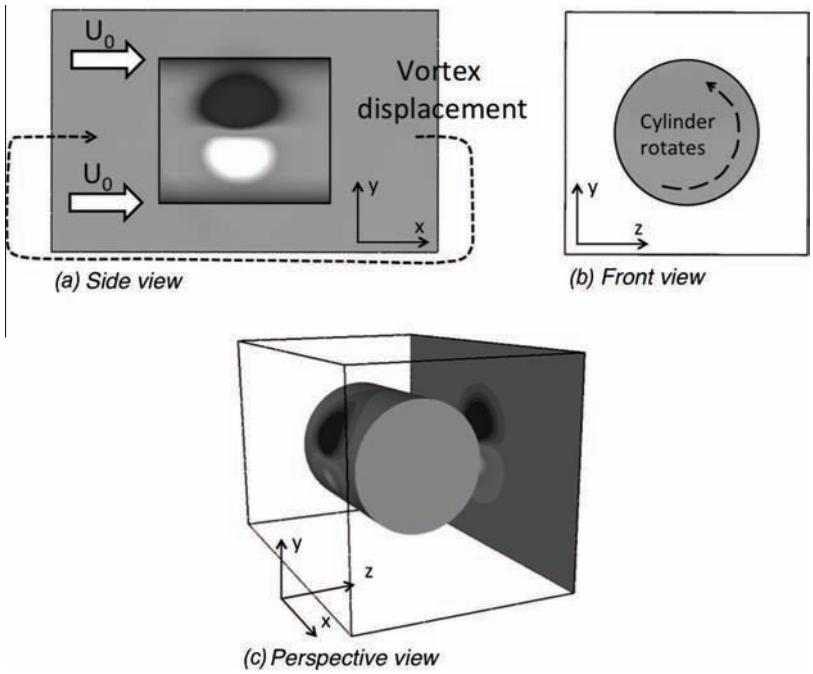

Fig. 2. Sketch of the 3D convection vortex test case: a rotating cylinder is placed inside a tri-periodic box. Views are colored by the velocity field.

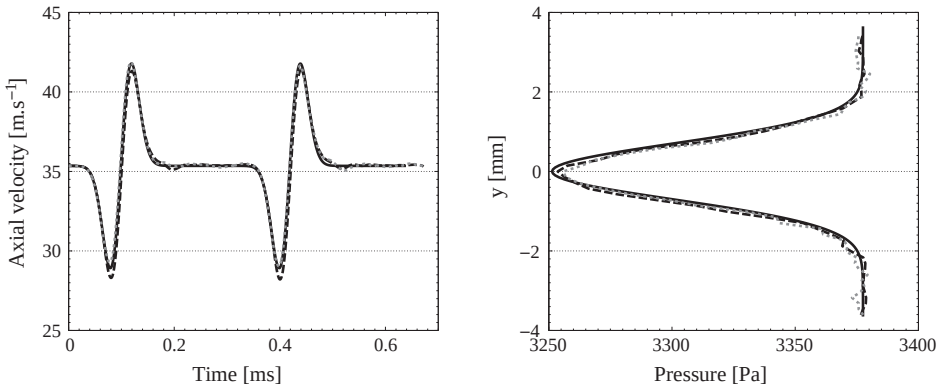

(a) Axial velocity at center of the cylinder versus time.

(b) Pressure along y-axis after two convection times.

Fig. 3. Comparison between a single domain AVBP computation and the MISCOG approach. ——: analytical solution; - - -: single mesh approach; ····: MISCOG.

4.2. Efficiency of the MISCOG approach

The load balancing of the MISCOG approach strategy raises much more questions than the usual optimization of single instance codes on parallel systems: the present configuration requires the coupling of 7 AVBP entities (one for the bomb and 6 six for the fans). Timers were added to measure the times needed for (1) computation, T_c, (2) exchange, T_e and (3) waiting, T_w.

Defining a waiting time T_w in a multiple instances run requires caution. Here we define T_w using the following convention: T_w is negative when fans (AVBP02–AVBP07) wait while it is positive if the bomb (AVBP01) waits. Note that T_e corresponds to exchanges between AVBP01 and individual fans: communication times between cores inside each instance are included in the computation time. Two computation times are defined: T_c^f and T_c^b, the fan and the bomb standalone computational times, respectively.

A theoretical model of performance for MISCOG can be derived using simple relations. Two limit cases are considered. The bomb-limited case (BL) where fans have to wait – corresponding to $T_w < 0$ – and the fan-limited case (FL) where the bomb has to wait – corresponding to $T_w > 0$ –. Timetables of BL and FL cases are displayed in Figs. 7 and 8, respectively. According to timetables presented in Figs. 7 and 8 and using the convention previously proposed for the waiting time, leads to an expression for T_w, which is valid for all cases:

$$T_w = (T_c^f - T_c^b) - (N-2)T_e \tag{3}$$

The exchange time, T_e, cannot be estimated simply (its dependance on load balancing is not easy to evaluate) and it was measured in the solver. The total time for one iteration T_{it} can be expressed using two relations: communications between instances in MISCOG approach are sequential so that (except for the first iteration) the time needed by the bomb (AVBP01) to compute one iteration T_{it}^b is equal to the time needed by each fan (AVBP02–AVBP07) to compute one iteration T_{it}^f (Figs. 7 and 8). This leads to two expressions for T_{it}:

$$T_{it} = \underbrace{(N-1)T_e + T_c^b + \max(0, T_w)}_{T_{it}^b} = \underbrace{T_e + T_c^f - \min(0, T_w)}_{T_{it}^f} \tag{4}$$

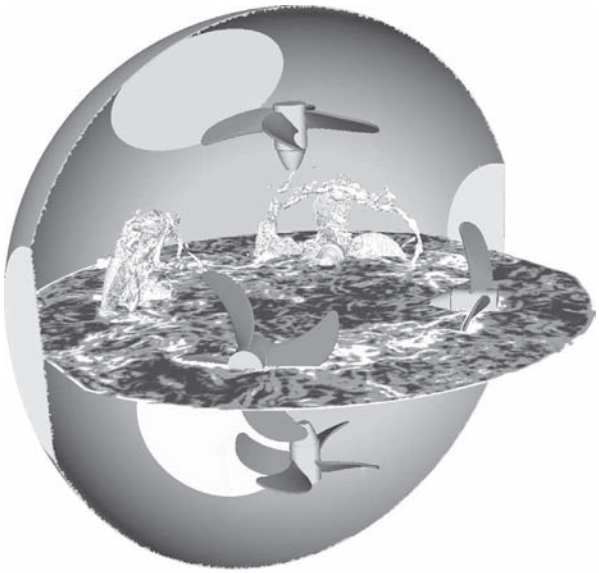

(a) Sketch of the geometry. $|\nabla \vec{u}|$ instantaneous field in the central plane and iso-surfaces of vorticity in fan regions (for 2 fans only).

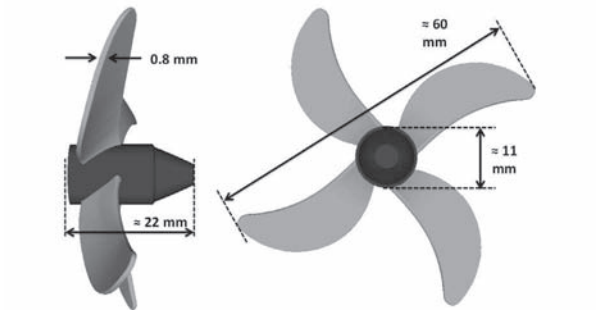

(b) Characteristics of the fan used to stir the vessel.

Fig. 4. Sketch of the geometry (top) and fan characteristics (bottom) (configuration setup at the PRISME laboratory, Orléans).

Table 1
Experimental data about the flow at the bomb center.

$\mathbf{u}_{\mathbf{rms},\mathrm{exp}}$	3 m/s
$L_{\tau,exp}$	3 mm
τ	1 ms
$Re_{t,exp}$	600
η_{exp}	40 μm

To validate this model, computations were performed where the total number of cores was fixed (400 on SGI Altix ICE 8200) and the ratio $R_c = N_c^b/N_c^f$ of the number of cores allocated to the bomb instance AVBP01 (N_c^b) to the number of cores allocated to fan instances AVBP02 to AVBP07 (N_c^f) was varied (all fan instances have the same number of cores). Table 2 summarizes the computations performed to evaluate the performance of MISCOG. Fig. 9 compares the model (Eqs. (3) and (4)) to waiting and total times measured in simulations. Fig. 9(a) shows the waiting times. When Rc is increased (more cores are allocated to the bomb instance AVBP01), the waiting time is expected to go from negative (fans wait) to positive (bomb waits) values as shown by Eq. (3). A good agreement is found while Rc is less than 20. For large Rc values, the trend is good but values differs slightly: in simulations the waiting time goes to zero but remains negative. When there are extreme differences in load balancing between AVBP01 and AVBP02 ($R_c > 20$) the behavior of MISCOG is not well understood yet. According to Eq. (3), in order to cancel the waiting time ($T_w = 0$), the load balancing must be chosen such as $T_c^f = T_c^b + (N-2)T_e$. This leads here to a ratio $Rc \simeq 19$, where 303 cores are allocated to AVBP01 (the bomb) and 16 cores are used for each fan domain. Fig. 9(b) displays the absolute execution time of the code for one time-iteration. The agreement with Eq. (4) is reasonable.

In an ideal computation, the minimum computing cost of such a simulation is obtained when $T_w = 0$. In practice, the R_c range which minimizes the total time for one iteration is $R_c \in [10; 20]$ showing that the MISCOG efficiency is weakly dependent on this ratio. In this range, T_w is closed to zero but can be negative showing that the optimal performance of MISCOG can be obtained in a situation where fans wait.

Fig. 6. y^+ field on the fan walls.

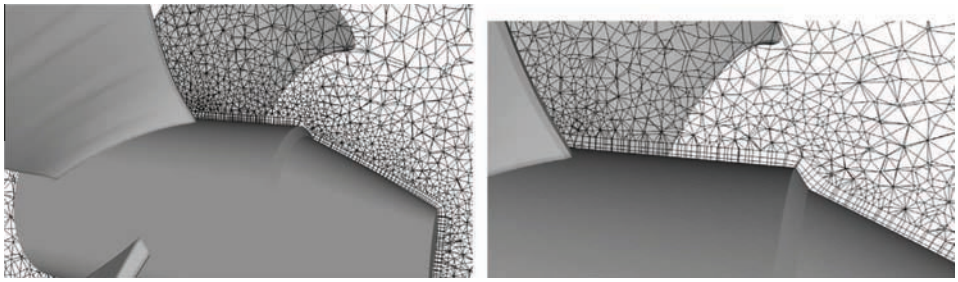

Fig. 5. Mesh of the fan. Four prism layers were added near blade-walls.

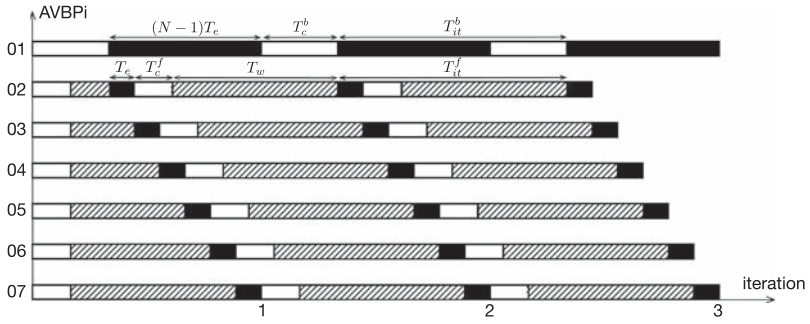

Fig. 7. Timetable of the operations performed in the MISCOG approach for the BL case (only fans wait). ▭: Computing; ▨: waiting; ▬: exchanging.

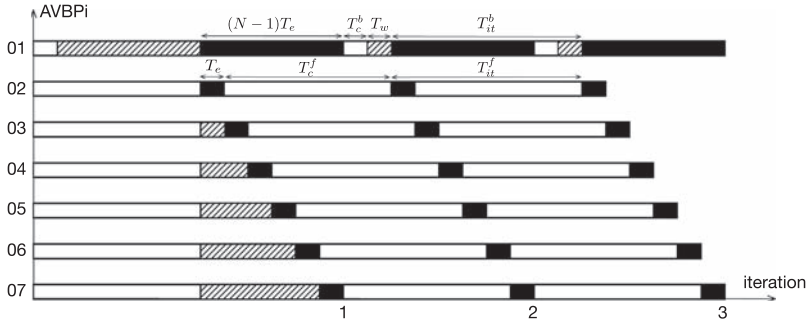

Fig. 8. Timetable of the operations performed in the MISCOG approach for the FL case (only bomb waits). ▭: Computing; ▨: waiting; ▬: exchanging.

Table 2
Simulations performed to evaluate the performance of MISCOG. The ratio R_c is increased for MISCOG 1–5. All times are given in seconds per iteration.

Name	R_c	T_e	T_w	T_{it}
MISCOG 1	2	0.593	−4.35	6.19
MISCOG 2	4.5	0.345	−2.42	4.37
MISCOG 3	9.9	0.347	−1.28	3.93
MISCOG 4	19	0.423	−0.34	4.03
MISCOG 5	34	0.606	−0.25	7.84

5. Characterization of turbulent flow inside the fan-stirred bomb

In the experimental set-up, many operating points have been studied: four fan geometries have been tested, the fan rotation speed ω_{fan} was varied from 1,000 rpm to 15,000 rpm, the pressure P_0 from 1 bar to 10 bar and the temperature T_0 from 323 K to 473 K. Only one operating point is studied numerically: $P_0 = 101325$ Pa and $T_0 = 323$ K. The fans rotation speed is $\omega_{fan} = 10,000$ rpm (the corresponding rotation period is $T_{fan} = 6$ ms). The Reynolds number, based on the blade tip radius (30 mm) and speed (31.5 m/s) is about 60,000. A normalized time t^* giving the number of fan rotations that are computed is defined as $t^* = t/T_{fan}$, where t is the physical time.

To reach steady state, a first computation is performed on a coarse grid. Fig. 10 shows the evolution of the mean resolved kinetic energy in the computational domain $E_k = 1/V \iiint_V \mathbf{u}^2 dV$. This quantity is a relevant diagnostic to quantify the temporal convergence of the flow inside the vessel. In this configuration, the flow is established after about 20 rotations. From $t^* = 0$–45, the LW scheme is used. Then from $t^* = 45$–95, the TTGC scheme is used. Finally from $t^* = 95$–165, the computation is performed on the fine grid with the TTGC scheme. The resolved mean kinetic energy E_k

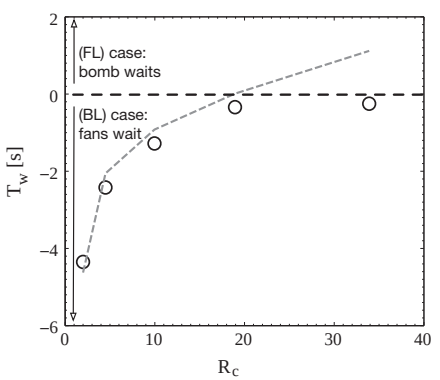

(a) Waiting time T_w.

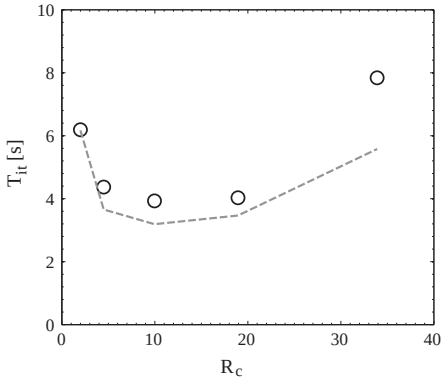

(b) Total time for one iteration T_{it}.

Fig. 9. Performance of MISCOG. ○: Computations; – – –: model.

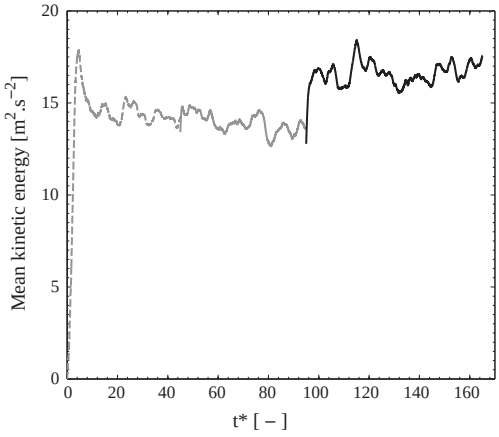

Fig. 10. Mean kinetic energy in the closed vessel versus the number of fan rotations t^*. – – – –: coarse grid LW; ———: coarse grid TTGC; ——: fine grid TTGC.

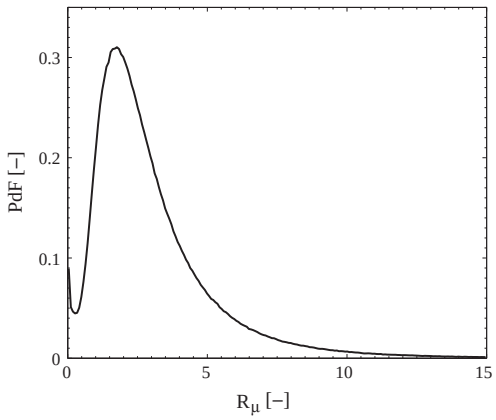

Fig. 11. Ratio R_μ of the turbulent viscosity μ_t on laminar viscosity $\mu_l : R_\mu = \mu_t/\mu_l$.

increases slightly when the fine grid is introduced because new structures are created. However the new steady state is reached quickly and diagnostics are performed from $t^* = 105$–165.

To check the quality of the LES, the ratio R_μ of turbulent viscosity μ_t (created by the subgrid-scale model) over laminar viscosity μ_l was computed: Fig. 11 shows a probability density function (PdF) of R_μ over all grid nodes. The maximum value of R_μ reaches 15 times the laminar viscosity but is much less at most points. This diagnostic shows that a large portion of the turbulence is resolved on the mesh and not modeled.

5.1. Velocity at the bomb center

Fig. 12 presents the temporal evolution of the three velocity components $\mathbf{u} = (u, v, w)$ at the center of the vessel. The signal recorded by the probe is zero until $t^* = 6$. This time represents the time needed by large turbulent scales generated by fans to reach the center of the vessel. The distance between the fan blades to the center of the vessel is $L_{fv} = 65$ mm. A velocity V_s can be estimated by the relation $V_s = L_{fv}/t^* \simeq 2$ m/s. This velocity is very small compared to the flow velocity at the blade tip $V_{bt} \simeq 30$ m/s. The mechanism by which turbulence goes from fan regions to the bomb center is described in Section 5.4.

The RMS velocity values[3] at the center of the vessel are respectively 2.3, 2.0 and 2.1 m/s. Probability density functions of

[3] The RMS values are defined as $u_{rms} = \sqrt{\sum_{n=1}^{Ns} u_n'^2/N_s}$ where N_s is the number of samples and $u' = u - \bar{u}$. They do not include the SGS contribution.

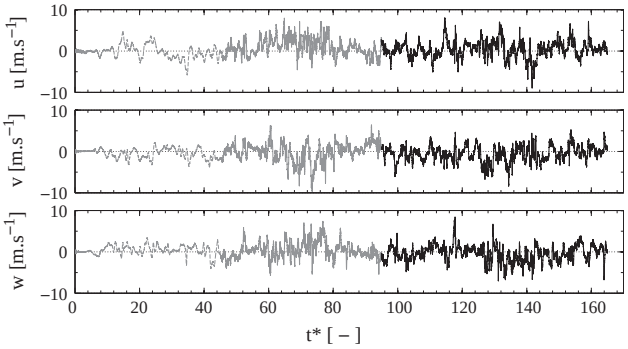

Fig. 12. Velocity components versus number of fan rotations t^* at the center of the vessel. – – – –: coarse grid LW; ———: coarse grid TTGC; ——: fine grid TTGC.

the velocity fluctuations components $\mathbf{u}'$ are plotted on Fig. 13. The pdf's of u', v' and w' are compared to a Gaussian distribution which characterizes random processes. A good agreement is found between a Gaussian distribution and the distribution of the velocity components at the bomb center. These first results suggest that turbulence at the center is close to HIT which is the objective of this experimental set-up.

5.2. Mean and RMS velocities in the closed vessel

A second diagnostic is to compare average $\bar{\mathbf{u}}$ and fluctuating $\mathbf{u}_{\mathbf{rms}}$ velocities measured experimentally to those computed by LES. These statistics are performed oven 60 fan rotations ($t^* \in [105; 165]$). Fig. 14 shows fields of the magnitude of the average and fluctuating velocities in the closed vessel. As expected, the average velocity is close to zero at the bomb center. To compare these results to experimental data, Fig. 15 presents x-axis cuts of average velocity components. As previously observed on Fig. 14, average velocities are near zero at the bomb center. The agreement between experimental data and LES calculation is reasonable. Moreover the 'S' shape of the $\bar{u}$ and $\bar{v}$ curves observed experimentally is fairly well predicted by the computation. The domain where the average velocity is near zero is a sphere with a radius of about 3 cm. Fig. 16 presents x-axis cuts of fluctuating velocities components. Once again the agreement between experimental data and LES is quiet good. The u_{rms} and v_{rms} profiles are well captured. The LES results slightly under-estimate the velocity fluctuations since only the resolved fluctuations are plotted. Considering the complexity of this simulation, capturing most of the trends observed in the measurements is already challenging and we think that results are sufficiently good to show that the whole approach is promising.

5.3. Turbulence structure

To study the structure of the turbulence, the time average invariants defined by Lumley [51,52] are a useful tool. According to this theory an anisotropy invariant map within which all realizable Reynolds stress invariants must lie can be defined. The borders of this domain describe different states of the turbulence. This theory is based on the analysis of the non-dimensional form of the anisotropy tensor given by:

$$b_{ij} = \frac{\overline{\tau_{ij}}}{\overline{\tau_{kk}}} - \frac{1}{3}\delta_{ij} \tag{5}$$

with $\overline{\tau_{ij}} = \overline{u_i' u_j'}$ the average Reynolds stress tensor. The principal components of the anisotropy tensor may be found by solving the relation:

$$\det[b_{ij} - \sigma\delta_{ij}] = 0. \tag{6}$$

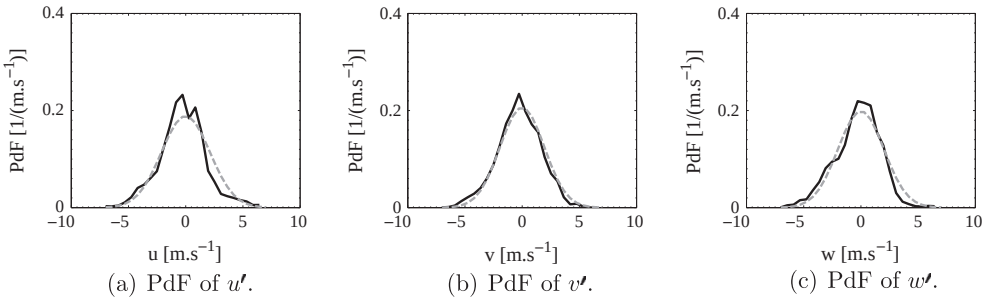

(a) PdF of u'. (b) PdF of v'. (c) PdF of w'.

Fig. 13. Local velocity fluctuations distributions at the bomb center. - - - -: Gaussian distribution; ——: LES.

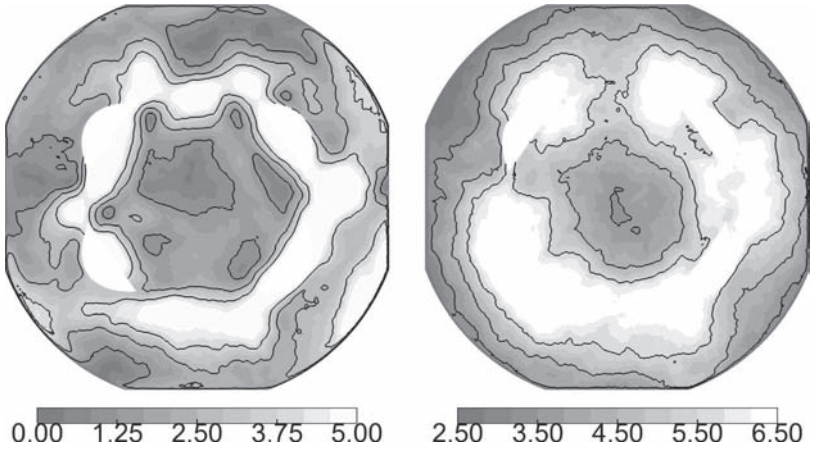

(a) Average velocity (modulus). (b) RMS velocity (modulus).

Fig. 14. Average and RMS velocity fields. (Statistics performed on 60 fan rotations, $t^* \in [105; 165]$.)

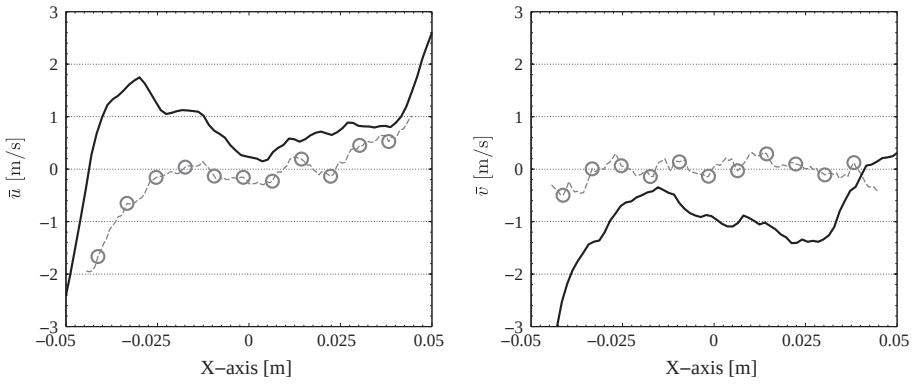

(a) $\bar{u}$. (b) $\bar{v}$.

Fig. 15. Comparison of the average velocities $\bar{u}$ and $\bar{v}$ along the x-axis. -⊖-: experimental data (PIV); ——: LES. (Statistics performed on 60 fan rotations, $t^* \in [105; 165]$.)

where σ are the eigenvalues (i.e. the principal stresses) of $\mathbf{b}$. Eq. (6) expands to the following third-order equation for:

$$\sigma^3 - I_1\sigma^2 + I_2\sigma - I_3 = 0 \tag{7}$$

where I_1, I_2 and I_3 are respectively the first, second, and third invariants of the tensor b_{ij}. These invariants are related to the tensor terms according to the relations:

$$\begin{aligned} I_1 &= \text{trace}(\mathbf{b}) = b_{kk} \\ I_2 &= \frac{1}{2}\left([\text{trace}(\mathbf{b})]^2 - \text{trace}(\mathbf{b^2})\right) = -\frac{1}{2}b_{ij}b_{ji} \\ I_3 &= \det(\mathbf{b}) \end{aligned} \tag{8}$$

I_1 is zero for incompressible flows and is not used here. The anisotropy invariant map is constructed by plotting $-I_2$ versus I_3. Isotropic turbulence is found at the origin ($I_2 = I_3 = 0$). When I_2 or I_3 differ from zero, they quantify the type of turbulence which is found locally (1, 2 or 3 components, axi-symmetry, etc.). The I_2 and I_3 invariants were computed locally (which means that the $\bar{\cdot}$ operator in Eq. (5) is a temporal averaging operator) in the LES on the fine mesh during the established phase ($t^* > 105$). This analysis has been done on the x, y and z-axis (20 points in each direction) of the closed vessel and results are reported in Fig. 17. Each point is colored by its distance r to the center of the bomb.

Fig. 17 shows that at the bomb center ($x \in [-30; +30]$ mm), turbulence can be assumed to be isotropic. In this spherical domain all

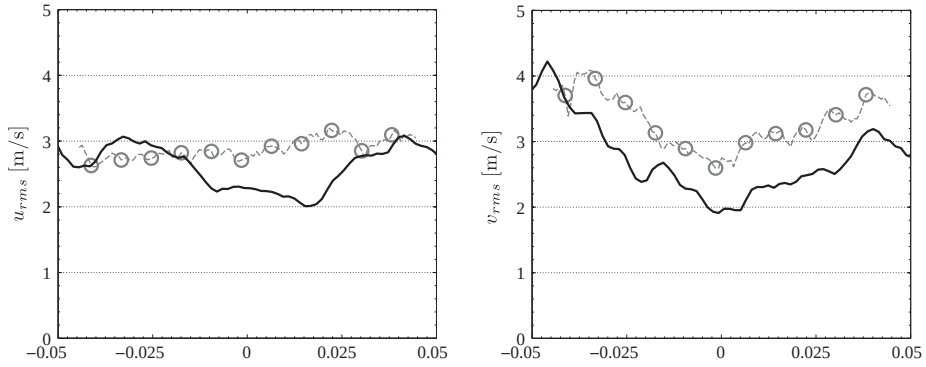

(a) u_{rms}. (b) v_{rms}.

Fig. 16. Comparison of the fluctuating velocities u_{rms} and v_{rms} along the x-axis. -⊖-: experimental data (PIV); ——: LES. (Statistics performed on 60 fan rotations, $t^* \in [105; 165]$.)

structures generated by the six fans impact and mix (by diffusion) leading to an homogenous turbulence. Outside this spherical domain where turbulence is isotropic, the presence of the fans affects the structure of the turbulence: at a distance of more than 30 mm of the bomb center, turbulence becomes 'rod-like'. This loss of isotropy is confirmed by results obtained experimentally. Fig. 18 presents the evolution of the ration u_{rms}/v_{rms} versus the x-axis showing that turbulence is isotropic at the bomb center. The agreement between LES and experimental measurements is good. Note that Fig. 18 is consistent with Fig. 17

5.4. Kinetic energy balance

The objective in this section is to show how turbulence is transferred from the fans regions to the bomb center. A relevant quantity to characterize the turbulence inside the vessel in terms of production, dissipation and transport is the mean turbulent kinetic energy (TKE) $\bar{e} = 1/2\overline{u_i' u_i'}$. The budget of $\bar{e}$ is given by Hinze [3]:

$$\underbrace{-\overline{u_i}\frac{\partial \bar{e}}{\partial x_i}}_{\text{Convection}} \underbrace{-\frac{\partial}{\partial x_i}\left(\overline{p' u_i'}\right)}_{\text{Pressure diffusion}} \underbrace{-\frac{\partial}{\partial x_i}\left(\overline{e u_i'}\right)}_{\text{Turbulent diffusion}} \underbrace{+\frac{\partial}{\partial x_j}\left(2\overline{(\nu+\nu_t)s_{ij}' u_i'}\right)}_{\text{Viscous diffusion}}$$
$$\underbrace{-2\overline{(\nu+\nu_t)s_{ij}' s_{ij}'}}_{\text{Dissipation}} \underbrace{-\overline{u_i' u_j'}\frac{\partial \overline{u_i}}{\partial x_j}}_{\text{Production}} = 0 \qquad (9)$$

where p' is the pressure fluctuation, e is the instantaneous turbulent kinetic energy $e = 1/2 u_i' u_i'$ and $s_{ij}' = 1/2\left(\partial u_i'/\partial x_j + \partial u_j'/\partial x_i\right)$ is the deformation tensor [53,4,54,55]. The turbulent viscosity $\nu_t = \mu_t/\rho$ is taken into account in the budget of $\bar{e}$. Terms in Eq. (9) are calculated over 60 solutions: 1 solution is stored at each fan rotation from $t^* = 105$ to $t^* = 165$. These solutions are uncorrelated since the time between two solutions is 6 ms and the time scale associated to the integral length scale τ is around 1 ms (convergence was checked). These terms are then averaged spatially assuming spherical symmetry so that they are plotted as a function of the bomb radius r_b ($r_b = 0$ at the bomb center). Only terms of interest are plotted here: Fig. 19 displays the convection, turbulent diffusion, dissipation and the production terms (resolved quantities). A fan is superimposed to the graph to show its position in the bomb. The dissipation rate found in this work is about 100 m^2/s^3 in the region of the bomb center. This value is in agreement with the dissipation rate measured experimentally by De Jong et al. [56] in an eight-fan cubic turbulence box. The production term is maximum at $r_b/R_0 \simeq 0.5$: the turbulent kinetic energy is produced by fans which are located at this position. Finally, over a central region of

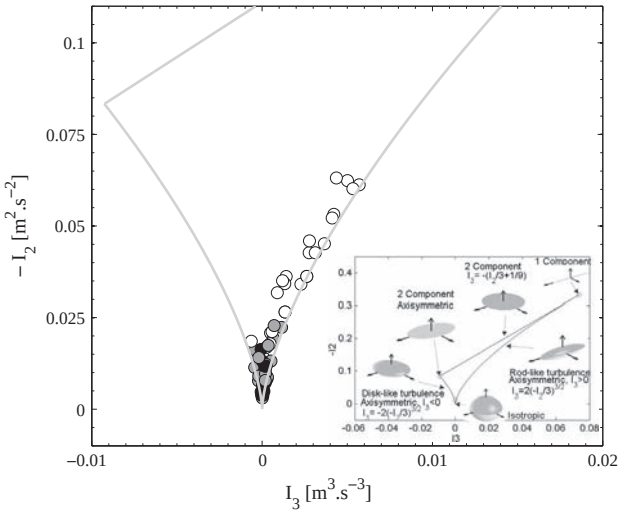

Fig. 17. Anisotropy invariant map (Lumley triangle). Each point is colored by its distance r to the center of the bomb. ●: $r < 15$ mm; ●: $r \in [15; 30]$ mm; ○: $r > 30$ mm. The figure in the bottom-right hand side is taken from [52].

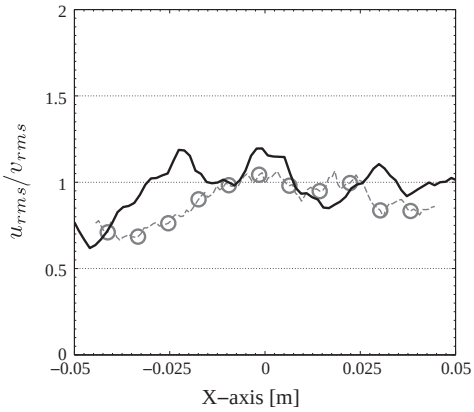

Fig. 18. Isotropy along the x-axis. -⊖-: experimental data (PIV); ——: LES. (Statistics performed on 60 fan rotations, $t^* \in [105; 165]$.)

diameter 30 mm, turbulent diffusion dominates convection as expected: the mean flow is around zero in this region (see Fig. 15), confirming that turbulence is not convected but diffused towards the bomb center from the fan regions.

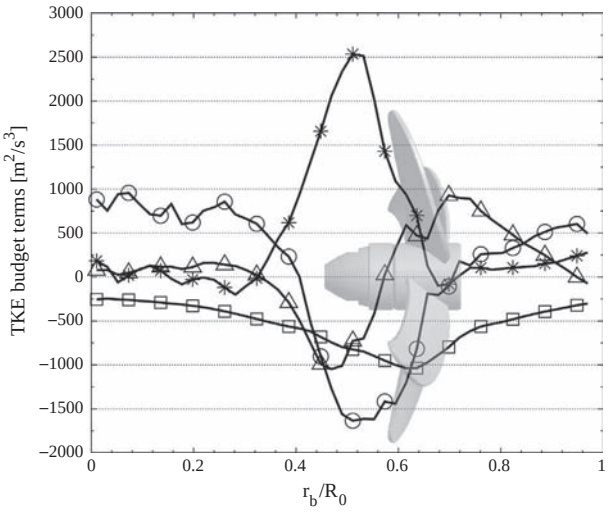

Fig. 19. Budget of resolved TKE terms versus the normalized bomb radius r_b/R_0. —◁—: Convection; —○—: turbulent diffusion; —□—: dissipation; —✳—: production.

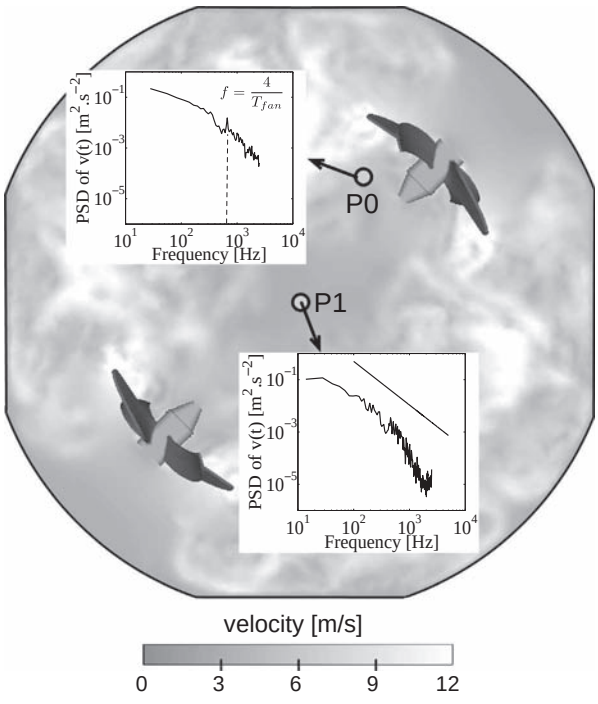

Fig. 20. Velocity spectra close to a fan and at the bomb center.

5.5. Spectra

The flow generated by fans is, by nature, a pulsating flow. Because fans have four blades, this flow is expected to exhibit a mode at a frequency f_p equal to four times the fan rotation frequency ($f_p = 4/T_{fan}$). To check if turbulence at the center of the bomb is affected by the pulsated flow created by the blades rotation, Power Spectral Density (PSD) of the velocity can be computed to track the existence of harmonic oscillations at f_p.

Fig. 20 shows the bomb configuration and the position where PSD are performed. Two points in the domain are analyzed: close to a fan (point P0) and at the bomb center (point P1). At P0, the PSD exhibits a mode at a frequency exactly equal to four times the frequency of the fan rotation as expected. On the other hand, at the bomb center, this mode vanishes and the spectrum follows the Kolmogorov theory [57]. Here the slope of the spectrum is near the −5/3 theoretical slope. This confirms that the turbulence at the bomb center is not affected by the periodicity of the flow generated by fans. Moreover, PSD results show that more energy is contained in the spectrum at point P0 than at point P1 (showing that turbulence decays between these two points).

6. Conclusion

This study presents a computation of a spherical vessel stirred by six fans. This configuration corresponds to an experiment conducted at the PRISME laboratory in Orléans to study the propagation of turbulent premixed flames in homogeneous isotropic turbulence. In this paper, only the non-reacting flow is studied, just before ignition. At this instant, the Reynolds number associated to the fans is 60,000 while the Reynolds number based on the integral length and RMS speed is of the order of 600 at the bomb center.

An approach first developed for turbomachinery simulations called MISCOG, has been adapted here to handle six fans inside the vessel. This method couples multiple instances of the same code, exchanging residuals on small overlapping zones. A first test case shows that the MISCOG approach is able to convect vortices with limited dispersion and dissipation effects. The parallel efficiency of MISCOG is discussed too.

A well resolved LES of the full geometry is then performed with the unstructured compressible code AVBP. Average and fluctuating fields match experimental data reasonably well. Finally the structure of the turbulence is studied and it is shown that turbulence is almost homogeneous and isotropic at the bomb center in a region of around 6 cm of diameter. The budget of mean turbulent kinetic energy is performed too and shows that turbulence is not convected from fans to the bomb center but diffused since the average velocities are near zero at this location. The trace of the blade passage frequency disappears near the bomb center.

Acknowledgments

Authors acknowledge F. Halter, F. Foucher and B. Galmiche from PRISME laboratory for their experimental results. This work was granted access to the high-performance computing resources of CINES under the allocation x20132b6607 made by Grand Equipement National de Calcul Intensif.

References

[1] Tennekes H. Simple model for the smallscale structure of turbulence. Phys Fluids 1968;11(3):669–70.
[2] Tennekes H, Lumley JL. A first course in turbulence. Cambridge: M.I.T. Press; 1972.
[3] Hinze JO. Turbulence. New-York: McGraw-Hill; 1975.
[4] Risso F, Fabre J. Diffusive turbulence in a confined jet experiment. J Fluid Mech 1997;337:233–61.
[5] Pope SB. Turbulent flows. Cambridge University Press; 2000.
[6] Sagaut P. Large eddy simulation for incompressible flows. Springer; 2002.
[7] Garnier E, Mossi M, Sagaut P, Comte P, Deville M. On the use of shock-capturing schemes for large-eddy simulation. J Comput Phys 1999;153(2):273–311.
[8] Lenormand E, Sagaut P, Phuoc LT, Comte P. Subgrid-scale models for large-eddy simulations of compressible wall bounded flows. AIAA J 2000;41(6):1340–50.
[9] Moin P, Squires KD, Cabot W, Lee S. A dynamic subgrid-scale model for compressible turbulence and scalar transport. Phys Fluids A 1991;3(11):2746–57.
[10] Mashayek F, Jaberi FA, Miller RS, Givi P. Dispersion and polydispersity of droplets in stationary isotropic turbulence. Int J Multiphase Flow 1997;23(2):337–55.
[11] Aliseda A, Cartellier A, Hainaux F, Lasheras JC. Effect of preferential concentration on the settling velocity of heavy particles in homogeneous isotropic turbulence. J Fluid Mech 2002;468:77–105.
[12] Salazar JPLC, De Jong J, Cao L, Woodward SH, Meng H, Collins LR. Experimental and numerical investigation of inertial particle clustering in isotropic turbulence. J Fluid Mech 2008;600:245–56.

[13] Birouk M, Gokalp I. Current status of droplet evaporation in turbulent flows. Prog Energy Comb Sci 2006;32(4):408–23.
[14] Poinsot T, Veynante D. Theoretical and numerical combustion, 3rd ed.; 2011 <http://www.cerfacs.fr/elearning>.
[15] Peters N. Turbulent combustion. Cambridge University Press; 2001.
[16] Girimaji SS, Pope SB. Propagating surfaces in isotropic turbulence. J Fluid Mech 1992;234:247–77.
[17] Laffitte P. La propagation des flammes dans les mélanges gazeux, Hermann et Cie. Actualités scientifiques et industrielles, Paris; 1939.
[18] Semenov E. Measurement of turbulence characteristics in a closed volume with artificial turbulence. Combust Expl Shock Waves 1965;1(2):57–62.
[19] Abdel-Gayed RG, Bradley D, Hamid MN, Lawes M. Lewis number effects on turbulent burning velocity. Proc Combust Inst 1984;20:505–12.
[20] Gulder O. Turbulent premixed flame propagation models for different combustion regimes. In: 23rd Symposium (International) on Combustion, vol. 23(1); 1991. p. 743–50.
[21] Chen JH, Im HG. Correlation of flame speed with stretch in turbulent premixed methane/air flames. In: 27th Symposium (International) on Combustion, vol. 1; 1998. p. 819–26.
[22] Shy SS, Lin WJ, Wei JC. An experimental correlation of turbulent burning velocities for premixed turbulent methane–air combustion. Proc R Soc Lond A 2000;456(2000):1997–2019.
[23] Liao S, Jiang D, Huang Z, Zeng K, Cheng Q. Determination of the laminar burning velocities for mixtures of ethanol and air at elevated temperatures. Appl Therm Eng 2007;27(2–3):374–80.
[24] Birouk M, Sarh B, Gökalp I. An attempt to realize experimental isotropic turbulence at low Reynolds number. Flow Turb Combust 2003;70(1–4):325–48.
[25] Hwang W, Eaton JK. Creating homogeneous and isotropic turbulence without a mean flow. Exp Fluids 2004;36(3):444–54.
[26] Brachet ME, Bustamante MD, Krstulovic G, Mininni PD, Pouquet A, Rosenberg D. Ideal evolution of MHD turbulence when imposing Taylor–Green symmetries. Phys Rev E 2013;87:1–16.
[27] Spalart PR, Moser RD, Rogers MM. Spectral methods for the Navier–Stokes equations with one infinite and two periodic directions. J Comput Phys 1991;96(2):297–324.
[28] Moser RD, Moin P, Leonard A. A spectral numerical method for the Navier–Stokes equations with applications to Taylor–Couette flow. J Comput Phys 1983;52(3):524–44.
[29] Lele S. Compact finite difference schemes with spectral like resolution. J Comput Phys 1992;103(1):16–42.
[30] Berland J, Bogey C, Marsden O, Bailly C. High-order, low dispersive and low dissipative explicit schemes for multiple-scale and boundary problems. J Comput Phys 2007;224(2):637–62.
[31] Marié S, Ricot D, Sagaut P. Comparison between lattice Boltzmann method and NavierStokes high order schemes for computational aeroacoustics. J Comput Phys 2009;228(4):1056–70.
[32] Moureau V. Simulation aux grandes échelles de l'aérodynamique interne des moteurs à piston. Ph.D. thesis, Ecole Centrale Paris; 2004.
[33] Moureau V, Barton I, Angelberger C, Poinsot T. Towards large eddy simulation in internal-combustion engines: simulation of a compressed tumble flow. In: SAE 113 (2004-01-1995); 2004. p. 1315–24.
[34] Moureau V, Lartigue G, Sommerer Y, Angelberger C, Colin O, Poinsot T. Numerical methods for unsteady compressible multi-component reacting flows on fixed and moving grids. J Comput Phys 2005;202(2):710–36.
[35] Peskin CS. The immersed boundary method. Acta Numer 2002:479–517.
[36] Verzicco R, Mohd-Yusof J, Orlandi P, Haworth D. Large eddy simulation in complex geometric configurations using boundary body forces. AIAA J 2000;38(3):427–33.
[37] Mittal R, Iaccarino G. Immersed boundary methods. Ann Rev Fluid Mech 2005;37(1):239–61.
[38] Wang G, Papadogiannis D, Duchaine F, Gourdain N, Gicquel LYM. Towards massively parallel large eddy simulation of turbine stages. In: ASME Turbo Expo 2013. San Antonio (TX), USA; 2013.
[39] Wang G, Moreau S, Duchaine F, Gourdain N, Gicquel LYM. Large eddy simulations of the MT1 high-pressure turbine using TurboAVBP. In: Proceeding of 21st annual conference of the CFD society of Canada. Sherbrooke, Quebec, Canada; 2013.
[40] Piacentini A, Morel T, Thévenin A, Duchaine F. Open-palm an open source dynamic parallel coupler. In: IV International conference on computational methods for coupled problems in science and engineering; 2011.
[41] Duchaine F, Jauré S, Poitou D, Quémerais E, Staffelbach G, Morel T, et al. High performance conjugate heat transfer with the OpenPALM coupler. In: V International conference on coupled problems in science and engineering – coupled problems. Ibiza, Spain; 2013.
[42] Galmiche B, Halter F, Mazellier N, Foucher F. Turbulent flow field measurements in a fan-stirred combustion vessel. In: European turbulence conference; 2013.
[43] Schønfeld T, Rudgyard M. Steady and unsteady flows simulations using the hybrid flow solver avbp. AIAA J 1999;37(11):1378–85.
[44] Lax PD, Wendroff B. Difference schemes for hyperbolic equations with high order of accuracy. Commun Pure Appl Math 1964;17:381–98.
[45] Colin O, Rudgyard M. Development of high-order Taylor–Galerkin schemes for unsteady calculations. J Comput Phys 2000;162(2):338–71.
[46] Hirt CW, Amsden A, Cook JL. An arbitrary Lagrangian–Eulerian computing method for all flow speeds. J Comput Phys 1974;131(4):371–85.
[47] Moureau VR, Vasilyev OV, Angelberger C, Poinsot TJ. Commutation errors in Large Eddy simulations on moving grids: application to piston engine flows. In: Proceedings of the summer program, center for turbulence research. NASA AMES/Stanford University, USA; 2004. p. 157–68.
[48] Enaux B, Granet V, Vermorel O, Lacour C, Pera C, Angelberger C, et al. Les and experimental study of cycle-to-cycle variations in a spark ignition engine. Proc Combust Inst 2011;33:3115–22.
[49] Ducros F, Nicoud F, Poinsot T. Wall-adapating local eddy-viscosity models for simulations in complex geometries. In: Baines MJ, editor. ICFD; 1998. p. 293–300.
[50] Boileau M, Duchaine F, Jouhaud J-C, Sommerer Y. Large-Eddy simulation of heat transfer around a square cylinder using unstructured grids. AIAA J 2013;51(2):372–85.
[51] Lumley J. Computational modelling of turbulent flows. Advan Appl Mech 1978;18:123–76.
[52] Simonsen AJ, Krogstad P-A. Turbulent stress invariant analysis: clarification of existing terminology. Phys Fluids 2005;17(8):088103.
[53] Dwyer MJ, Patton EG, Shaw RH. Turbulent kinetic energy budgets from a large-eddy simulation of airflow above and within a forest canopy. Bound-Layer Meteorol 1997;84(1):23–43.
[54] Liu X, Thomas FO. Measurement of the turbulent kinetic energy budget of a planar wake flow in pressure gradients. Exp Fluids 2004;37(4):469–82.
[55] Sideridis A, Yakinthos K, Goulas A. Turbulent kinetic energy balance measurements in the wake of a low-pressure turbine blade. Int J Heat Fluid Flow 2011;32(1):212–25.
[56] De Jong J, Cao L, Woodward SH, Salazar JPLC, Collins LR, Meng H. Dissipation rate estimation from PIV in zero-mean isotropic turbulence. Exp Fluids 2008;46(3):499–515.
[57] Kolmogorov AN. The local structure of turbulence in incompressible viscous fluid for very large reynolds numbers. C R Acad Sci, USSR 1941;30:301.